Oxidative Stress by Ca^{2+} Overload is Critical for Phosphate-Induced Vascular Calcification

Nhung Thi Nguyen[1,2], Tuyet Thi Nguyen[1,3,#], Dat Da Ly[1,2], Jing-Bo Xia[4], Xu-Feng Qi[4], In-Kyu Lee[5], Seung-Kuy Cha[1,2], Kyu-Sang Park[1,2,#]

[1]Department of Physiology, [2]Mitohormesis Research Center, Yonsei University Wonju College of Medicine, Wonju, Korea, [3]Internal Medicine Residency Program, College of Health Sciences, Vin University, Hanoi, Vietnam, [4]Key Laboratory of Regenerative Medicine, Ministry of Education, Department of Developmental and Regenerative Biology, Jinan University, Guangzhou, China, [5]Department of Internal Medicine, School of Medicine, Kyungpook National University, Daegu, Korea

Running Head: ROS by Ca^{2+} overload in vascular calcification

[#] Correspondences:

Tuyet Thi Nguyen, M.D., Ph.D.

Internal Medicine Residency Program, College of Health Sciences, Vin University,

Times City, 458 Minh Khai, Hai Ba Trung Dist, Hanoi, Vietnam

Tel: +84-24-7-108-9779, Email: v.tuyetnt10@vingroup.net

Kyu-Sang Park, M.D., Ph.D.

Department of Physiology, Yonsei University Wonju College of Medicine,

Wonju, 26426, Republic of Korea,

Tel: +82-33-741-0294, Fax: +82-33-745-6461, Email: qsang@yonsei.ac.kr

Manuscript Type: Original Research

Word counts: total main text 5,209 words including Abstract (249 words), New & Noteworthy (75 words), Introduction (514 words), Materials and Methods (1,894 words), Results (1,159 words), Discussion (1,318 words)

49 references, 6 figures, 4 supplementary figures, 1 supplementary table.

ABSTRACT

Hyperphosphatemia is the primary risk factor for vascular calcification, which is closely associated with cardiovascular morbidity and mortality. Recent evidence showed that oxidative stress by high inorganic phosphate (Pi) mediates calcific changes in vascular smooth muscle cells (VSMCs). However, intracellular signalings responsible for Pi-induced oxidative stress remain unclear. Here, we investigated molecular mechanisms of Pi-induced oxidative stress related with intracellular Ca^{2+} ($[Ca^{2+}]_i$) disturbance, which is critical for calcification of VSMCs. VSMCs isolated from rat thoracic aorta or A7r5 cells were incubated with high Pi-containing medium. Extracellular signal-regulated kinase (ERK) and mammalian target of rapamycin were activated by high Pi that was required for vascular calcification. High Pi upregulated expressions of type III sodium-phosphate cotransporters, PiT-1 and -2, and stimulated their trafficking to the plasma membrane. Interestingly, high Pi increased $[Ca^{2+}]_i$ exclusively dependent on extracellular Na^+ and Ca^{2+} as well as PiT-1/2 abundance. Furthermore, high Pi induced plasma membrane depolarization mediated by PiT-1/2. Pretreatment with verapamil, as a voltage-gated Ca^{2+} channel (VGCC) blocker, inhibited Pi-induced $[Ca^{2+}]_i$ elevation, oxidative stress, ERK activation and osteogenic differentiation. These protective effects were reiterated by extracellular Ca^{2+} free condition, intracellular Ca^{2+} chelation or suppression of oxidative stress. Mitochondrial superoxide scavenger also effectively abrogated ERK activation and osteogenic differentiation of VSMCs by high Pi. Taken together, we suggest that high Pi activates depolarization-triggered Ca^{2+} influx via VGCC, and subsequent $[Ca^{2+}]_i$ increase elicits oxidative stress and osteogenic differentiation.

PiT-1/2 mediates Pi-induced $[Ca^{2+}]_i$ overload and oxidative stress, but in turn, PiT-1/2 is upregulated by consequences of these alterations.

Keywords: Hyperphosphatemia; Oxidative stress; Calcium overload; Voltage-gated calcium channel; Type III sodium-phosphate cotransporters; Vascular calcification

NEW & NOTEWORTHY

The novel findings of this study are PiT-1/2-dependent depolarization by high Pi, leading to Ca^{2+} entry via voltage-gated Ca^{2+} channel in vascular smooth muscle cells. Cytosolic Ca^{2+} increase and subsequent oxidative stress are indispensable for osteogenic differentiation and calcification. In addition, plasmalemmal abundance of PiT-1/2 relies on Ca^{2+} overload and oxidative stress, establishing a positive feedback loop. Identification of mechanistic components of vicious cycle could provide novel therapeutic strategies against vascular calcification in hyperphosphatemic patients.

Abbreviations

CKD, chronic kidney diseases; Pi, inorganic phosphate; $[Ca^{2+}]_i$- intracellular Ca^{2+} concentration, VSMCs, vascular smooth muscle cells; Runx2, runt-related transcription factor 2; OPN, osteopontin; ER- Endoplasmic reticulum; ROS, reactive oxygen species; $\Delta\Psi_p$, plasma membrane potential; $\Delta\Psi_m$, mitochondrial membrane potential; ERK, extracellular signal-regulated kinase; mTOR, mammalian Target of Rapamycin; NF-κR, nuclear factor kappa-light-chain-enhancer of activated B cells; VGCCs, voltage-gated Ca^{2+} channels; NAC, N-acetyl-L-cysteine; EGTA-AM, ethylene glycol-bis (β-aminoethyl ether)-N,N,N′,N′-tetraacetic acid-acetoxymethyl ester; mtTP, mitoTEMPO; PI3K, phosphatidylinositol-3-kinase

INTRODUCTION

Hyperphosphatemia is closely associated with a variety of complications, including vascular calcification (14, 21), cardiovascular event (38, 40), metabolic diseases and aging (23, 27). In chronic kidney disease (CKD), defective inorganic phosphate (Pi) excretion leads to vascular calcification, a serious complication that contributes to high rates of morbidity and mortality (19, 41, 44). Remarkably, prospective cohort studies reveal that, even in individuals without CKD, high serum Pi concentration within the normal range significantly correlates with the prevalence of cardiovascular disease and diabetes mellitus (16, 18).

Medial arterial calcification, frequently found in CKD patients with elevated serum Pi, is primarily caused by trans-differentiation of vascular smooth muscle cells (VSMCs) into osteoblast-like cells (10). This reprogramming is followed by apoptosis-dependent matrix mineralization (24, 35), decreased availability of calcification inhibitors and remodelling of the extracellular vascular matrix (24, 34). Notably, several early studies have focused on the role of sodium-phosphate cotransporters (NaPi) in the pathogenesis of high Pi-induced vascular calcification (25, 43). NaPi transporters are divided into three families, type I, II and III, based on structure, tissue expression and biochemical characteristics (39). Type III NaPi (PiT-1 and -2) transporter is proposed as the predominant route for cellular Pi uptake in vascular smooth muscle and essential for Pi-elicited osteogenic/chondrogenic phenotype change as well as matrix mineralization (7). Knockdown of PiT-1 and -2 significantly diminished expression of the osteogenic differentiation markers, Runt-related transcription factor 2 (Runx2) and osteopontin (OPN), and reduced vascular calcification by high Pi both *in vitro* and *in vivo* (7). However, functional

consequences of plasmalemmal Pi transport, including cellular signaling cascades, has not been clearly elucidated.

Available evidence suggests that elevated Ca^{2+} is linked to plaque thickness in CKD patients and vascular calcification (32, 46). However, studies have concentrated on the serum Ca^{2+} level, independent of Pi action. Impacts of high Pi on intracellular Ca^{2+} concentration ($[Ca^{2+}]_i$) and whether impaired $[Ca^{2+}]_i$ homeostasis can initiate detrimental signaling to develop calcification are not well investigated. Particularly, the pathological connection between Ca^{2+} overload and oxidative stress, which may play an important role in the pathogenesis of vascular calcification, would be interesting but have not clarified yet.

Previous studies in insulin-secreting cells have demonstrated that high Pi exposure upregulates PiT-1 and PiT-2 expression and causes cytosolic alkalinization. This increase in intracellular pH facilitates Pi transport into the mitochondrial matrix and subsequently accelerates superoxide production, mitochondrial permeability transition, endoplasmic reticulum (ER) stress and defective insulin secretion (27, 28). The critical role of mitochondrial reactive oxygen species (ROS) in high Pi-induced vascular calcification was proposed in the study by Zhao et al., suggesting that ROS-mediated mitochondria-to-nucleus signaling occurs via the nuclear factor-κB (NF-κB) pathway (1). Notably, Pi-induced mitochondrial ROS generation is related to mitochondrial Pi uptake and alterations in mitochondrial membrane potential ($\Delta\Psi_m$) (28).

In this study, we demonstrated that high extracellular Pi increased protein expressions and surface traffickings of PiT-1 and PiT-2 in vascular smooth muscle cells. Intriguingly, high Pi elevated $[Ca^{2+}]_i$ via voltage-gated Ca^{2+} entry triggered by

depolarization of plasma membrane potential ($\Delta\Psi_p$). This $[Ca^{2+}]_i$ increase by high Pi was responsible for oxidative stress and calcification in vascular smooth muscle.

MATERIALS AND METHODS

Chemicals

Krebs-Ringer bicarbonate buffer solution contains: 5.5 mM glucose; 0.5 mM $MgSO_4$; 3.6 mM KCl; 0.5 mM NaH_2PO_4; 2 mM $NaHCO_3$; 140 mM NaCl; 10 mM HEPES; and pH 7.4 adjusted with NaOH. Most of chemicals and drugs including ethylene glycol-bis (β-aminoethyl ether)-N,N,N′,N′-tetraacetic acid-acetoxymethyl ester (EGTA-AM), rapamycin, and catalase were purchased from Sigma-Aldrich (St. Louis, MO, USA). UO126 and wortmannin were purchased from Tocris Bioscience (Bristol, UK). Wogonin was obtained from Cayman chemicals (Ann Arbor, MI, USA).

Isolation of primary vascular smooth muscle cells and cell culture

Using a protocol for tissue explant, primary VSMCs were isolated from thoracic aortas of six-week-old male Sprague Dawley rats (150–200g, DBL, Eumseong, Korea), as described previously (30). Briefly, we anaesthetized rats with an intraperitoneal injection of ketamine (80 mg/kg) and xylazine (40 mg/kg). Then, thoracic aortas were removed and transferred to cell culture dishes. Explants were left undisturbed for 4–5 days. After 5−7 days, cells began to migrate from the edges of tissue blocks. Once cells achieved confluence, primary VSMCs were transferred into 60 mm cell culture dishes. VSMCs were maintained in a humidified atmosphere (37°C) containing 5% CO_2 in complete Dulbecco's Modified Eagle Medium (DMEM) medium (Hyclone, Themo Fisher Scientific, Waltham, MA, USA, #HY-SH30243.01) supplemented with 10% Fetal Bovine Serum (FBS) (Gibco, Themo Fisher Scientific, #16000-044), 100 U/ml penicillin and 100ug/ml streptomycin (Hyclone, #SV30010).

All procedures were performed in compliance with the guidelines of the Institutional Animal Care and Use Committee (IACUC) at Yonsei University, Wonju College of Medicine (YWC-180424-1). A7r5 cells, a clonal cell line of rat aortic vascular smooth muscle, were commercially obtained from ATCC (CRL-1444) and maintained in DMEM medium supplemented with 10% FBS, 1% penicillin and streptomycin. A7r5 cells were used from passage 11 to 25. To induce calcification, pVSMCs and A7r5 cells were incubated in DMEM medium containing high Pi (3mM and 5mM) for 2 days. All the inhibitors including UO126 (10μM), rapamycin (10nM), EGTA-AM (2μM), NAC (3mM), mtTP (100nM), verapamil (10μM), Wogonin (5μM) were preincubated into cells 1h prior to Pi treatment.

Alizarin staining

Primary VSMCs and A7r5 cells were fixed with 4% paraformaldehyde after incubating in calcific medium, and then washed three times with phosphate-buffered saline (PBS). Cells were incubated with 2% Alizarin red (ScienCell, Carlsbad, CA, USA, #223, pH = 4.1~4.3 with 10% ammonium hydroxide or 1M HCl) for 30 min. Cells were washed with distilled water. For quantitative analysis, DMSO were added on stained cells to dissolve Alizarin and the absorbance (450 nm) of supernatant was measured by microplate spectrophotometer (Epoch, Bio-Tek, Winooski, VT, USA).

Quantitative reverse transcription-polymerase chain reaction (RT-PCR)

Total RNAs were extracted from VSMCs using a Hybrid-R^{TM} total RNA purification kit (GeneAll, Seoul, Korea, #305-101). The quality of RNA was confirmed by

examining ratios of spectrophotometry at 260 nm and 280 nm. Reverse transcription of total RNA was performed by using a ReverTra Ace (Toyobo, Osaka, Japan, # FSQ301). Quantitative RT-PCR used an Applied Biosystems QuantStudio 6 Flex Real-Time PCR system and SYBR Green (AB Bioscience, Concord, MA, USA, #AB4367659). Primer sequences are listed in Supplementary Table 1. All PCR runs were repeated three times and PCR data were analyzed using the delta-delta-CT method with β-actin as an internal reference.

Western blotting and cell surface biotinylation assay

Primary VSMCs and A7r5 cells seeded on six-well plates were harvested, washed with PBS three times and lysed with cold RIPA buffer (Pierce, Waltham, MA, USA, #89900). Lysate buffer contained phosphatase inhibitor cocktail (Roche, Basel, Switzerland, #4906837001) and protease inhibitor (Roche, #4693159001). After centrifugation at 13,000 rpm for 20 min, supernatant was collected without disturbing cell pellets. Protein levels in supernatants were measured using a BCA kit (Pierce, #23223). Supernatants were then loaded onto SDS-PAGE and subsequently transferred to polyvinylidene difluoride membranes (Merk Milipore, Billerica, MA, USA, #IPH00010). Membranes were blocked with 6% skim milk or 5% BSA for 1 h at room temperature. After blocking, membranes were washed twice with 0.1% TBST and incubated with primary antibodies overnight at 4 ˚C: p-PERK (Cell signaling, Danvers, MA, USA, #4370P); t-ERK (Cell signaling, #9102); p-p70S6K (Cell signaling, #9205S); p70S6K (Cell signaling, #9202); PiT-1 (Proteintech Group, Chicago, IL, USA, #12423-I-AP) and PiT-2 (Santa Cruz Biotechnology, Dallas, TX, USA, #sc-68420), β-Actin (Abcam, Cambridge, MA, USA, #ab6276), p-PERK (Cell

signaling, #3179), t-PERK(Cell signaling, #3192) and CHOP (Cell signaling, #2895), then with secondary anti-rabbit (Invitrogen, Carlsbad, CA, USA, #31460) or anti-mouse HRP-conjugated antibodies (Invitrogen, #31450) for 1 h at room temperature. Antibodies were detected by using ECL detection reagent (Amersham, Little Chalfont, UK, #RPN2235/2232). Each band was quantified with ImageJ software and results are shown as the ratio of total protein to β-actin and phosphorylated protein to β-actin normalised to controls.

For biotinylation assay, A7r5 cells seeded on 100 mm dishes were washed twice with ice-cold Ca^{2+}-Mg^{2+}-free PBS. Then, cells were incubated with biotinylation solution with 1.5 mg/ml Sulfo-NHS-SS-Biotin (Pierce, #21331) overnight at 4 ˚C. Next, quenching buffer was added into cells and incubated on shaker for 20 min. Then, cells were washed twice and lysed with ice-cold lysis buffer containing phosphatase inhibitor cocktail (Roche, #4906837001) and protease inhibitor (Roche, #4693159001). Supernatant of cell lysate was mixed with streptavidin agarose resin beads (Thermo Scientific, Cat.no # 20353) and rotated for 1h at 4 ˚C. The mixture was centrifuged at 6,000 rpm for 10 min and washed with ice-cold Triton X-100-Tris-buffered saline (140 mM NaCl, 10nM Tris-HCl pH 7.4, 5mM KCl, 1% Triton X-100). Harvested protein including total and biotinylated proteins were then loaded onto SDS-PAGE with similar steps in western blotting.

Cell viability and apoptotic assay

For checking cell viability, VSMCs were placed at 10^4 cells/well in a 96-well plate. UO126 and rapamycin were pretreated for 1 h prior to 48 h co-incubation with 5 mM

Pi. MTT solution was prepared by dissolving 3-[4,5-dimethylthiazol-2-yl]-2,5-diphenyl tetrazolium bromide (Sigma-Aldrich, #M2128) in fresh DMEM medium at 0.5 mg/ml. After indicated treatment, cells were incubated with 100 μL of MTT solution in incubator for 2 h. After removing medium, DMSO was added into each well to dissolve formazan and gently shake for 10 min. The absorbance was measured at 570 nm by Epoch^{TM} Microplate Spectrophometer (Bio-Tek, Winooski, VT).

To detect apoptosis, the amount of DNA fragmentation in VSMCs were quantified using ELISA assay (Cell Death Detection ELISA Plus kit, Roche Diagnostics, #11774425001). 10^4 cells were placed in 96-well plate. After high Pi treatment with or without UO126/rapamycin, cells were washed twice with warm PBS and added 200 μL of lysis buffer provided in the kit to each well, and incubated for 30 min at room temperature. After centrifugation, 20 μL supernatant was used for the reactions following steps in the protocol of manufacturer.

Intracellular calcium measurement

A7r5 cells were seeded onto 12 mm L-poly-lysine coated coverslips (15,000 cells/coverslip). To measure $[Ca^{2+}]_i$, cells were incubated with 5 μM Fura-2 (Invitrogen, #F1221) in darkness for 40 min at room temperature. After incubation, cells were washed five times with buffer. Images were continuously captured every 10 s using an IX-73 inverted microscope (Olympus, Tokyo, Japan) equipped with a camera system (Prime-BSI CMOS camera; Photometrics, USA). Cells were excited at 340 and 380 nm and emission was detected at 510 nm using MetaFlour 6.1 (Molecular Devices, San Jose, CA, USA). The F_{340}/F_{380} ratio reflects $[Ca^{2+}]_i$. As an

alternative method, cells seeded on black-walled 96-well plates with 5,000 cells/well were loaded with Fura-2 for 40 min at room temperature. F_{340}/F_{380} ratios were measured using a multi-well fluorescence reader (FlexStation II, Molecular Devices).

Plasma membrane potential measurement

Plasma membrane potential ($\Delta\Psi_p$) was measured using $DiBAC_4(3)$ (Invitrogen, #B438). Briefly, cells were seeded onto 12 mm L-poly-lysine coated coverslips and incubated with 200 nM $DiBAC_4(3)$ in darkness for 30 min. Coverslips were then placed in the chamber and fixed to the inverted microscope (Olympus) with camera (Photometrics). The fluorophore was excited at 490 nm and emitted fluorescence was measured at 520 nm. Data were corrected by background subtraction and analyzed using MetaFluor software (Molecular Devices).

Cytosolic and mitochondrial ROS measurement

Cytosolic ROS was measured using DCF-DA (Invitrogen, #D399). Primary VSMCs or A7r5 cells were seeded onto 15 mm coverslips and loaded with 2.5 μM DCF-DA in normal KRB for 15 min at 37 ˚C. Then, cells were washed twice and fluorescent images (excitation/emission: 488/530 nm) were collected using the inverted microscope (Olympus) with camera (Photometrix). All the images were analyzed using MetaMorph software and each data set was originated from at least three independent experiments.

As an alternative method, cells seeded on black-walled 96-well plates with 10,000

cells/well were loaded with DCF-DA for 15 min at room temperature. The fluorescence intensity was measured using a multi-well fluorescence reader (FlexStation II, Molecular Devices).

Mitochondrial superoxide generation was measured using mitoSOX (Invitrogen, #M36008), a red fluorescent dye which carries a positive charge and localizes in mitochondria. Cells were loaded with 5 μM mitoSOX for 20 min at 37 ˚C and washed twice with normal KRB. Fluorescent images (excitation/emission: 510/580 nm) were collected and analyzed by the same as described above.

Mitochondrial membrane potential measurement

Mitochondrial membrane potential ($\Delta\Psi_m$) was measured using the fluorescent dye, JC-1 (Invitrogen, #T3168) in permeabilized cells. Cells were seeded on black-walled 96-well flexStation plates with 2×10^4 cells/well. After incubation, cells were washed twice, then loaded with JC-1 (300 nM) for 30 min at 37 ˚C. Cells were then permeabilized using Staphylococcus aureus α-toxin (Sigma, #H9395) in intracellular buffer solution (140 mM KCl, 5 mM NaCl, 7 mM $MgSO_4$, 1 mM KH_2PO_4, 1.65 mM $CaCl_2$, 10.2 mM EGTA, 20 mM HEPES, pH 7.0). Mitochondrial membrane potential was determined based on the ratio of red (540 nm excitation and 590 nm emission) over green (490 nm excitation and 540 nm emission) fluorescence intensity. These ratios were measured using a multi-well fluorescence reader (FlexStation II, Molecular Devices).

Small interfering RNA transfection

To knockdown slc20a1 (PiT-1) and slc20a2 (PiT-2), SiGENOME Smartpool siRNA duplexes were purchased from Bioneer (Daejeon, Korea). Transfection of siRNA was carried out using DharmaFECT-1 siRNA transfection reagent (Thermo Fisher Scientific, #T-2001-03). Briefly, cells were seeded into 6-well plates with 5×10^4 cells/well and treated with siRNA (10 nM) with DharmaFECT-1 in Opti-MEM media (Gibco, #31985-070) based on manufacturer's instruction. Knockdown efficiencies of PiT-1 and -2 were assessed by western blotting at 72 h after siRNA transfection.

Immunofluorescence staining

VSMCs were cultured onto 12 mm coverslips and incubated with Pi for 48 h. Cells were then washed twice with cold PBS and fixed with ice-cold 100% methanol for 15 min at room temperature. Cells were permeabilized with 0.1% Triton X/PBS for 10 min and incubated with 5% normal goat serum/PBS for 1 h at room temperature. After blocking, cells were incubated overnight at 4 ˚C with polyclonal anti-NF-κB p65 antibody (1:50 dilution; Santa Cruz, #sc-8008) followed by incubation with secondary antibody, Alexafluor 488 goat anti-mouse IgG (1:100 dilution, Invitrogen, #A-11001). Then, cells were counterstained with 1 μg/ml 4′,6′-diamidino-2-phenylindole (DAPI; Invitrogen, #D1306) for 5 min and mounted on a glass slide. Fluorescence images were obtained by using a confocal laser-scanning microscope (LSM 800; Zeiss, Oberkochen, Germany). A negative control was prepared using all the above steps, except incubation with primary antibody.

Statistical analysis

All values in the text and figures are expressed as mean ± standard deviation (SD) or standard error of the mean (SEM). The statistical analysis was performed by Student's *t*-test or one-way analysis of variance (ANOVA), followed by Turkey's multiple comparison test. *P*-values less than 0.05 were considered significant.

RESULTS

High phosphate activates ERK1/2-mTOR signaling and induces vascular calcification

To investigate the molecular mechanism involved in medial calcification, we first examine the effect of Pi on calcification of primary VSMCs isolated from rat aorta and A7r5 cells. In VSMCs, Ca^{2+} precipitation was increased by high Pi in a concentration-dependent manner (Figure 1A). As an intracellular signaling, extracellular signal-regulated kinase (ERK) was phosphorylated in calcifying VSMCs by high Pi. Moreover, p70S6K, a known downstream of mammalian target of rapamycin (mTOR), was also phosphorylated by high Pi in a pattern similar to ERK1/2 (Figure 1B and S1). Nuclear factor kappa-light-chain-enhancer of activated B cells (NF-κB) is reported to translocate into nuclei and activate osteoblastic differentiation of VSMCs (1). As expected, confocal images showed that immunofluorescence of NF-κB is mainly localized in nuclei under high Pi incubation (Figure 1C). Pre-treatment of a MEK/ERK inhibitor, UO126, or a mTOR inhibitor, rapamycin, effectively prevented Pi-induced osteogenic genes' upregulation (Figure 1D). Furthermore, rapamycin effectively inhibited ER stress markers, PERK and CHOP, elicited by high Pi (Figure 1E) and pretreatment of VSMCs with UO126 or rapamycin significantly reduced cytotoxicity and apoptotic DNA fragmentation after elevated Pi incubation (Figure 1F). Finally, pretreatment with UO126, rapamycin and a NF-κB inhibitor, wogonin, all repressed high Pi-induced vascular calcification to a considerable degree (Figure 1G,1H, and 1I).

Elevated phosphate increases expression of PiT-1/-2 and their surface trafficking

PiT-1 and PiT-2 are required for Pi-induced osteogenic differentiation and calcification of VSMCs (7). In CKD mice, high Pi diet increased mRNA levels of PiT-1 and calcification in the medial layer of aorta (26). We observed that PiT-1 expression was the most abundant among NaPi cotransporters in primary VSMCs and A7r5 cells, which was followed by PiT-2 (Figure 2A and S2). Incubation of A7r5 cells with high Pi-containing medium increased protein levels of PiT-1 and -2, which could promote additional Pi uptake into the cytoplasm (Figure 2B and 2C). Since mTOR is important for translational regulation, effects of ERK and mTOR inhibitors on PiT-1/2 upregulation were assessed. Notably, UO126 and rapamycin completely blocked PiT-1/2 protein upregulation by high Pi (Figure 2D and 2E). Interestingly, short exposure (< 1 h) of high Pi markedly promoted cell surface trafficking of PiT-1 via Ca^{2+}-dependent mechanism (Figure 2F, 2G, and S3). This translocation of PiT-1 into plasma membrane facilitates Pi uptake into cytosol soon (< 15 min) after an increase in extracellular Pi. Knockdown of PiT-1/2 showed protection against Pi-induced vascular calcification, further demonstrating the pathophysiologic impact of PiT-1/2 abundance in the development of vascular calcification (Figure 2H).

High phosphate increases cytosolic Ca^{2+} which is critical for vascular calcification

We investigated whether extracellular Pi affects cellular Ca^{2+} homeostasis by measuring $[Ca^{2+}]_i$ in VSMCs. Exposure to high Pi rapidly induced a considerable

increase of $[Ca^{2+}]_i$ (Figure 3A). These $[Ca^{2+}]_i$ changes were tightly dependent on extracellular Ca^{2+} concentration over a range of 0 to 1.8 mM, implying that $[Ca^{2+}]_i$ rise originates from the external source (Figure 3B). In the absence of extracellular Ca^{2+} or after chelation of cytosolic Ca^{2+} by EGTA-AM, ERK1/2 activation by Pi was abolished (Figure 3C). Moreover, extracellular Ca^{2+} free medium or pre-treatment of EGTA-AM prevented transcriptional upregulation of Runx2 and OPN (Figure 3D), as well as calcification of vascular smooth muscle (Figure 3E). These results indicate an essential role of $[Ca^{2+}]_i$ increase on intracellular signaling responsible for high Pi-induced osteogenic differentiation.

High phosphate depolarizes plasma membrane potential and triggers voltage-gated Ca^{2+} influx

VSMCs express different kinds of Ca^{2+} uptake routes, including L-type and N-type voltage-gated channels (VGCC) (Figure S4) (15). In general, opening of VGCC is preceded by $\Delta\Psi_p$ depolarization. Changes of $\Delta\Psi_p$ were therefore assessed using the membrane potential-sensitive fluorescence dye, $DiBAC_4(3)$. Fluorescence intensity was well correlated with changes of $\Delta\Psi_p$ induced by increasing extracellular K^+ concentration based on Nernst equation (Figure 4A). Intriguingly, elevating extracellular Pi concentration from 1 to 5 mM induced depolarization of $\Delta\Psi_p$ (Figure 4B), consistent with the previous observation of net inward current through PiT-1 (28). Moreover, knockdown of PiT-1 only or both PiT-1 and -2 eliminated Pi-induced $\Delta\Psi_p$ depolarization, demonstrating an exclusive role of PiT-1/2 in Pi-induced depolarization (Figure 4C). PiT-1 mediates Na^+ influx along with Pi and intracellular Na^+ increases by high extracellular Pi concentrations (28). Pi-induced $[Ca^{2+}]_i$ change

triggered by $\Delta\Psi_p$ depolarization also relies on Na^+ uptake since the increase in $[Ca^{2+}]_i$ by high Pi was absent in extracellular Na^+ free medium in which N-methyl-D-glutamine (NMDG) replaced Na^+ (Figure 4D). In addition, silencing of PiT-1/2 also completely inhibited Pi-triggered $[Ca^{2+}]_i$ increase (Figure 4E). Importantly, pre-incubation of VSMCs with a VGCC inhibitor, verapamil (10 μM), largely blocked Pi-induced increases in $[Ca^{2+}]_i$ (Figure 4F), reflecting an essential role of VGCC in Pi-induced Ca^{2+} influx. Verapamil also effectively inhibited high Pi-induced ERK1/2 activation as well as osteogenic differentiation of VSMCs via preventing upregulations of Runx2 and OPN (Figure 4G and 4H). Similarly, other osteogenic genes including alkaline phosphatase (ALP), Osterix, SRY-Box Transcription Factor 9 (Sox9) and Msh homeobox 2 (Msx2) were regulated by Pi-induced Ca^{2+} influx via VGCC (Figure S5). Consequently, pre-treatment of verapamil showed a substantial reduction in Pi-elicited vascular calcification (Figure 4I).

Oxidative stress by high Pi is dependent on increased cytosolic Ca^{2+}

Alteration in $[Ca^{2+}]_i$ homeostasis may cause cellular stress including augmentation of ROS production (42). In insulin-secreting cells, Pi elicits significant oxidative stress both in cytosol and mitochondria (27). Incubation of A7r5 cells in high Pi concentrations, in this study, triggered cytosolic ROS production, which was blocked by pre-treatment with N-acetylcysteine (NAC) or catalase (Figure 5A, 5B, figure S6A). Ca^{2+} free or EGTA-AM-containing medium prevented cytosolic ROS production, demonstrating an exclusive role of $[Ca^{2+}]_i$ on high Pi-induced oxidative stress (Figure 5C, 5D and figure S6B, S6C). Blockade of VGCC with verapamil also abolished ROS production by high Pi, consistent with its inhibitory effect on $[Ca^{2+}]_i$ changes (Figure

5E and figure S6D). The critical role of oxidative stress on vascular calcification was confirmed by pre-incubation with NAC, which entirely abolished high Pi-induced ERK activation (Figure 5F), upregulation of osteogenic genes (Figure 5G and S5) and calcium deposition in VSMCs (Figure 5H).

A mitochondrial superoxide scavenger prevents Pi-induced vascular calcification

In insulin-secreting cells, mitochondrial superoxide generation triggered by $\Delta\Psi_m$ hyperpolarization is involved in high Pi-induced permeability transition pore opening and apoptosis (27). In VSMCs, Pi also elicited $\Delta\Psi_m$ hyperpolarization in permeabilized cells (Figure 6A). Mitochondrial superoxide production was chased using mitoSOX with different time points of Pi incubation and achieved the highest status at around 6 h (Figure 6B). A mitochondrial ROS scavenger, mitoTEMPO (mtTP), was pre-treated before Pi incubation, which completely suppressed mitochondrial superoxide generation (Figure 6C) and partly reduced cytosolic ROS production (Figure S6E). Oxidative stress is an inducer for the nuclear translocation of NF-κB that initiates osteogenic gene transcription and osteoblast differentiation. Pre-incubation with mtTP effectively blunted NF-κB translocation into nuclei, ERK activation and PiT-1 upregulation in VSMCs by high Pi (Figure 6D and E). Consequently, Runx2 and OPN upregulation and calcification were also significantly inhibited by pre-treatment of mtTP (Figure 6F and G).

DISCUSSION

Vascular calcification is a serious complication of hyperphosphatemic patients with renal failure. However, molecular mechanisms of Pi actions are less understood, which limit development of successful preventive or therapeutic strategies for treating vascular calcification. In the present study, we demonstrated for the first time that high Pi triggers cytosolic Ca^{2+} influx via VGCC opened by membrane depolarization. Furthermore, the exclusive role of Ca^{2+} overload in Pi-induced oxidative stress leads to the signal activation and osteogenic differentiation, which also has not been reported yet. High Pi accelerates vascular calcification by increasing total protein expression of PiT-1 and -2 and their trafficking to the plasma membrane. Additionally, ERK activation and PiT-1/2 upregulation by Pi-induced oxidative stress engages pathogenic positive feedback loops that are crucial for significant calcific changes. All these mechanisms could provide novel therapeutic targets for the prevention and treatment of vascular calcification.

The molecular mechanism underlying ERK and mTOR activation by high Pi is not yet clear. In a kinetic study, ERK1/2 and p70S6K as a downstream of mTOR reached peak values around at 6 h of high Pi exposure and continued till at 24 h (Figure 1B). However, transient activations of ERK1/2 and mTOR were detected at the earlier time point, consistent with the previous report by Beck *et al*. (2). Early phosphorylation of ERK1/2 could be a consequence of membrane-delimited signaling, as part of the proposed Raf/MEK/ERK pathway activated by fibroblast growth factor receptors (47). Delayed ERK activation might be explained by different sensing mechanisms, for instance, induction of early genes such as *c-Fos* and *Egr-1*

464 *(5)*. In particular, oxidative stress is an important activator of early gene response,
465 which takes place within several hours of stimulus (20). Compatible with findings of
466 previous studies, both inhibitors of ERK signaling (UO126) and of mTOR (rapamycin)
467 prevent osteogenic gene upregulation and calcification (29, 37, 48). Therefore, Pi-
468 induced ROS generation is suggested to participate in delayed activations of ERK
469 and mTOR and subsequent calcific changes.

470 Among membrane phosphate transporters, PiT-1 and -2 are dominant for Pi uptake
471 in primary VSMCs and A7r5 cells. Similar to previous observations in other tissues,
472 high Pi exposure increases expression of PiT-1/2 that causes greater uptake of
473 extracellular Pi (28, 49). Intriguingly, both the total protein levels and cell surface
474 abundance of PiT-1/2 were augmented. Such changes further accelerate the
475 detrimental effects of Pi, worsening calcification. Although detailed regulatory
476 mechanisms for PiT-1/2 cell surface trafficking were not fully explored, previous
477 works show that phosphatidylinositol-4,5-biphosphaye 3-kinase (PI3K) modulates
478 intracellular vesicle trafficking via phosphorylation of its major downstream enzyme,
479 PKB/AKT (3, 45). As expected, high Pi rapidly stimulated phosphorylation of AKT at
480 serine and threonine sites and wortmannin, a PI3K inhibitor, completely blocked PiT-
481 1 cell surface trafficking (Figure S3A-C). Free Ca^{2+} medium also blocked PiT-1
482 surface trafficking suggesting that Ca^{2+} takes part in this upregulation (Figure S3D).

483 The essential roles of ERK and mTOR activation in PiT-1/2 upregulation are
484 demonstrated using signal inhibitors, UO126 and rapamycin. We infer that sequential
485 activation of ERK and mTOR after Pi treatment may participate in the development
486 of vascular calcification, which has been provide as an important pathogenic
487 mechanism of glomerular disease (9). Additionally, activation of mTOR by high Pi

488 facilitates ER stress responses, such as PERK phosphorylation and CHOP
489 upregulation, which were blocked by rapamycin. Increased CHOP, a pro-apoptotic
490 signal for ER stress, leads to Pi-induced apoptosis, as similarly observed in insulin-
491 secreting cells (27). Apoptotic bodies released from VSMCs accelerate extracellular
492 calcium phosphate crystal formation and deposition (31).

493 An interesting finding of this study is that high Pi triggers Ca^{2+} influx by opening
494 VGCCs, thus eliciting $[Ca^{2+}]_i$ increase in VSMCs. Indeed, sustained $[Ca^{2+}]_i$ elevation
495 by perfusion with a high Pi solution is dependent on extracellular Ca^{2+} and Pi
496 concentrations. Moreover, prevention of Ca^{2+} influx or $[Ca^{2+}]_i$ chelation completely
497 blocks ERK activation, oxidative stress, osteogenic differentiation and calcification.
498 Recent work by Robenbeck *et al.* provides evidence that $[Ca^{2+}]_i$ in VSMCs is
499 significantly elevated in concert with the progression of CKD in rats (33). The present
500 result may provide the mechanism for the higher level of $[Ca^{2+}]_i$ in a CKD model. In
501 VSMCs, L-type VGCC is the most important Ca^{2+} influx route (13). An appropriate
502 concentration of verapamil (10 μM), known to selectively block L-type VGCC,
503 successfully repressed the effect of Pi on $[Ca^{2+}]_i$ increase. The main activating
504 stimulus for VGCC-mediated Ca^{2+} influx is the depolarization of $\Delta\Psi_p$. Indeed, high Pi
505 exposure consistently depolarizes $\Delta\Psi_p$ that is responsible for opening VGCC.

506 In this study, an exclusive role of PiT-1 and -2 in Pi-induced depolarization and
507 subsequent activation of Ca^{2+} influx was demonstrated. Based on previous
508 electrophysiologic data in PiT-1-expressing HEK-293 cells, Pi concentration-
509 dependently elicits a net inward current, leading to membrane depolarization (28).
510 The inward current caused by Pi influx disappeared in a Na^+ free medium because of
511 cotransport with Na^+ (28). We suggest that movement of Na^+ and Pi via PiT-1/2

512 elicits $\Delta\Psi_p$ depolarization and $[Ca^{2+}]_i$ increase. This mechanism explains why
513 knockdown of PiT-1/-2 abolished both membrane potential depolarization and Ca^{2+}
514 influx by high Pi. The functional properties of PiT-1/2 were characterised by Forster
515 *et al.* in oocytes from *Xenopus laevis* and showed that PiT-1 preferentially transports
516 monovalent Pi ($H_2PO_4^-$) with two Na^+ (11, 12). This stoichiometric interpretation
517 seems consistent with the current hypothesis of total inward transport of cation.
518 However, previous observation demonstrated that Pi-induced inward current via PiT-
519 1 was less pronounced under pH 6.6 compared with pH 7.0 or 7.4. At this acidic
520 environment (pH 6.6), the monovalent form of Pi should be more dominant than
521 divalent form (HPO_4^{2-}), since the pKa between $H_2PO_4^-$ and HPO_4^{2-} is 7.2. To date,
522 this issue remains unresolved and further investigation is required.

523 Increased $[Ca^{2+}]_i$ in VSMCs leads to vascular contraction but also initiates
524 transcriptional regulation for reprogramming to a non-contractile phenotype (22). In
525 this work, increased $[Ca^{2+}]_i$ was tightly coupled with ROS generation. Interaction
526 between ROS and Ca^{2+} is considered bidirectional, wherein Ca^{2+} is likely pivotal for
527 ROS generation, while ROS can control cellular Ca^{2+} signaling (17). As another
528 consequence of $[Ca^{2+}]_i$ rise, it is conceivable that mitochondrial Ca^{2+} could be
529 increased due to more Ca^{2+} uptake from cytosol. This elevation of matrix Ca^{2+} may
530 stimulate mitochondrial metabolism and subsequently accelerate ROS generation (4).
531 Remarkably, Pi-induced hyperpolarization of $\Delta\Psi_m$ is shown to be followed by
532 mitochondrial superoxide production, consistent with previous reports in insulin-
533 secreting cells (27). Pharmacologic inhibition of mitochondrial Pi uptake reduced
534 $\Delta\Psi_m$ hyperpolarization and oxidative stress induced by high Pi (27, 28). Thus,
535 mitochondrial superoxide generation by high Pi may originate from alterations in

mitochondrial Ca^{2+} and $\Delta\Psi_m$ that collectively contribute to pathogenic cellular oxidative stress.

Oxidative stress deactivates the inhibitor of κB (IκBα), allowing NF-κB translocation to nuclei. Transcriptional activation by nuclear NF-κB upregulates osteogenic genes, which play crucial roles in calcific changes. Present data imply that Ca^{2+} overload and oxidative stress elicited by excessive Pi are responsible for ERK1/2 activation, since Pi-induced ERK1/2 phosphorylation is abolished by lowering either $[Ca^{2+}]_i$ (verapamil, EGTA-AM and Ca^{2+} free medium) or ROS (NAC and mtTP). Also, the essential role of ERK activation mediated by PiT-1 is reported to induce VSMC trans-differentiation under calcifying conditions (6, 36). However, higher $[Ca^{2+}]_i$ with calmodulin can directly activate Ras/Raf/ERK signaling, as described previously (8). The connection between Ca^{2+} and ERK signaling requires further investigation.

In conclusion, our study provides that aberrant Ca^{2+} influx by membrane depolarization is responsible for oxidative stress and osteogenic differentiation by high Pi in vascular smooth muscle. Further, pathologic positive feedback loops among Ca^{2+} overload, ROS generation, ERK-mTOR activation and an abundance of Pi transporters are critical in Pi-induced calcification. The identification of this vicious cycle suggests that blocking any step in this process could be effective against vascular calcification in hyperphosphatemic patients. Additionally, suppression of $\Delta\Psi_m$ hyperpolarization and superoxide generation could be effective strategies which have not yet been investigated. Identification of mitochondrial Pi transporters and their downstream consequences responsible for vascular calcification is necessitated for the development of novel therapeutic approaches.

Funding

This work was supported by the Medical Research Center Program (2017R1A5A2015369) and NRF Grant (2016R1A2B4014565) from Ministry of Science, ICT, and the R&D Project through the KHIDI (HI18C2196) from the Ministry of Health & Welfare, Korea.

Disclosures

The authors declare that they have no conflict of interest related to this work.

REFERENCES

1. **Al-Aly Z.** Phosphate, oxidative stress, and nuclear factor-κB activation in vascular calcification. *Kidney Int* 79: 1044-1047, 2011. doi:https://doi.org/10.1038/ki.2010.548.
2. **Beck GR, Jr., Knecht N.** Osteopontin regulation by inorganic phosphate is ERK1/2-, protein kinase C-, and proteasome-dependent. *J Biol Chem* 278: 41921-41929, 2003. doi:10.1074/jbc.M304470200.
3. **Bhattacharya S, McElhanon KE, Gushchina LV, Weisleder N.** Role of phosphatidylinositol-4,5-bisphosphate 3-kinase signaling in vesicular trafficking. *Life Sci* 167: 39-45, 2016. doi:10.1016/j.lfs.2016.10.018.
4. **Brookes PS, Yoon Y, Robotham JL, Anders MW, Sheu SS.** Calcium, ATP, and ROS: a mitochondrial love-hate triangle. *Am J Physiol Cell Physiol* 287: C817-833, 2004. doi:10.1152/ajpcell.00139.2004.
5. **Camalier CE, Yi M, Yu LR, Hood BL, Conrads KA, Lee YJ, Lin Y, Garneys LM, Bouloux GF, Young MR, Veenstra TD, Stephens RM, Colburn NH, Conrads TP, Beck GR, Jr.** An integrated understanding of the physiological response to elevated extracellular phosphate. *J Cell Physiol* 228: 1536-1550, 2013. doi:10.1002/jcp.24312.
6. **Chavkin NW, Chia JJ, Crouthamel MH, Giachelli CM.** Phosphate uptake-independent signaling functions of the type III sodium-dependent phosphate transporter, PiT-1, in vascular smooth muscle cells. *Exp Cell Res* 333: 39-48, 2015. doi:10.1016/j.yexcr.2015.02.002.
7. **Crouthamel MH, Lau WL, Leaf EM, Chavkin NW, Wallingford MC, Peterson DF, Li X, Liu Y, Chin MT, Levi M, Giachelli CM.** Sodium-dependent phosphate

592 cotransporters and phosphate-induced calcification of vascular smooth muscle
593 cells: redundant roles for PiT-1 and PiT-2. *Arterioscler Thromb Vasc Biol* 33:
594 2625-2632, 2013. doi:10.1161/atvbaha.113.302249.
595 8. **Cullen PJ, Lockyer PJ.** Integration of calcium and RAS signalling. *Nat Rev Mol*
596 *Cell Biol* 3: 339-348, 2002. doi:10.1038/nrm808.
597 9. **Das R, Kim SJ, Nguyen NT, Kwon HJ, Cha SK, Park KS.** Inhibition of the
598 ERK1/2-mTORC1 axis ameliorates proteinuria and the fibrogenic action of
599 transforming growth factor-β in Adriamycin-induced glomerulosclerosis. *Kidney*
600 *Int* 96: 927-941, 2019. doi:10.1016/j.kint.2019.05.006.
601 10. **Durham AL, Speer MY, Scatena M, Giachelli CM, Shanahan CM.** Role of
602 smooth muscle cells in vascular calcification: implications in atherosclerosis and
603 arterial stiffness. *Cardiovasc Res* 114: 590-600, 2018. doi:10.1093/cvr/cvy010.
604 11. **Forster IC, Hernando N, Biber J, Murer H.** Phosphate transport kinetics and
605 structure-function relationships of SLC34 and SLC20 proteins. *Curr Top Membr*
606 70: 313-356, 2012. doi:10.1016/b978-0-12-394316-3.00010-7.
607 12. **Forster IC, Hernando N, Biber J, Murer H.** Phosphate transporters of the
608 SLC20 and SLC34 families. *Mol Aspects Med* 34: 386-395, 2013.
609 doi:https://doi.org/10.1016/j.mam.2012.07.007.
610 13. **Ghosh D, Syed AU, Prada MP, Nystoriak MA, Santana LF, Nieves-Cintron M,**
611 **Navedo MF.** Calcium Channels in Vascular Smooth Muscle. *Adv Pharmacol* 78:
612 49-87, 2017. doi:10.1016/bs.apha.2016.08.002.
613 14. **Giachelli CM.** The emerging role of phosphate in vascular calcification. *Kidney*
614 *Int* 75: 890-897, 2009. doi:10.1038/ki.2008.644.
615 15. **Gollasch M, Haase H, Ried C, Lindschau C, Morano I, Luft FC, Haller H.** L-

type calcium channel expression depends on the differentiated state of vascular smooth muscle cells. *FASEB J* 12: 593-601, 1998. doi:10.1096/fasebj.12.7.593.

16. **Gonzalez-Parra E, Tuñón J, Egido J, Ortiz A.** Phosphate: a stealthier killer than previously thought? *Cardiovasc Pathol* 21: 372-381, 2012. doi:https://doi.org/10.1016/j.carpath.2012.02.008.
17. **Gordeeva AV, Zvyagilskaya RA, Labas YA.** Cross-talk between reactive oxygen species and calcium in living cells. *Biochemistry (Mosc)* 68: 1077-1080, 2003. doi:10.1023/a:1026398310003.
18. **Håglin L, Törnkvist B, Bäckman L.** Prediction of all-cause mortality in a patient population with hypertension and type 2 DM by using traditional risk factors and serum-phosphate,-calcium and-magnesium. *Acta Diabetol* 44: 138-143, 2007. doi:10.1007/s00592-007-0254-6.
19. **Hruska KA, Mathew S, Lund R, Qiu P, Pratt R.** Hyperphosphatemia of Chronic Kidney Disease. *Kidney Int* 74: 148-157, 2008. doi:10.1038/ki.2008.130.
20. **Jin N, Hatton ND, Harrington MA, Xia X, Larsen SH, Rhoades RA.** H(2)O(2)-induced egr-1, fra-1, and c-jun gene expression is mediated by tyrosine kinase in aortic smooth muscle cells. *Free Radic Biol Med* 29: 736-746, 2000. doi:10.1016/s0891-5849(00)00376-2.
21. **Komaba H, Fukagawa M.** Phosphate-a poison for humans? *Kidney Int* 90: 753-763, 2016. doi:10.1016/j.kint.2016.03.039.
22. **Kudryavtseva O, Aalkjær C, Matchkov VV.** Vascular smooth muscle cell phenotype is defined by Ca2+-dependent transcription factors. *FEBS J* 280: 5488-5499, 2013. doi:10.1111/febs.12414.
23. **Kuro-o M.** Klotho, phosphate and FGF-23 in ageing and disturbed mineral

640 metabolism. *Nat Rev Nephrol* 9: 650, 2013. doi:10.1038/nrneph.2013.111.
641 24. **Lanzer P, Boehm M, Sorribas V, Thiriet M, Janzen J, Zeller T, St Hilaire C,**
642 **Shanahan C.** Medial vascular calcification revisited: review and perspectives.
643 *Eur Heart J* 35: 1515-1525, 2014. doi:10.1093/eurheartj/ehu163.
644 25. **Li X, Yang HY, Giachelli CM.** Role of the sodium-dependent phosphate
645 cotransporter, Pit-1, in vascular smooth muscle cell calcification. *Circ Res* 98:
646 905-912, 2006. doi:10.1161/01.RES.0000216409.20863.e7.
647 26. **Mizobuchi M, Ogata H, Hatamura I, Koiwa F, Saji F, Shiizaki K, Negi S,**
648 **Kinugasa E, Ooshima A, Koshikawa S, Akizawa T.** Up-regulation of Cbfa1 and
649 Pit-1 in calcified artery of uraemic rats with severe hyperphosphataemia and
650 secondary hyperparathyroidism. *Nephrol Dial Transplant* 21: 911-916, 2005.
651 doi:10.1093/ndt/gfk008.
652 27. **Nguyen TT, Quan X, Hwang KH, Xu S, Das R, Choi SK, Wiederkehr A,**
653 **Wollheim CB, Cha SK, Park KS.** Mitochondrial oxidative stress mediates high-
654 phosphate-induced secretory defects and apoptosis in insulin-secreting cells. *Am*
655 *J Physiol Endocrinol Metab* 308: E933-941, 2015.
656 doi:10.1152/ajpendo.00009.2015.
657 28. **Nguyen TT, Quan X, Xu S, Das R, Cha SK, Kong ID, Shong M, Wollheim CB,**
658 **Park KS.** Intracellular alkalinization by phosphate uptake via type III sodium-
659 phosphate cotransporter participates in high-phosphate-induced mitochondrial
660 oxidative stress and defective insulin secretion. *FASEB J* 30: 3979-3988, 2016.
661 doi:10.1096/fj.201600455RR.
662 29. **Panda DK, Bai X, Sabbagh Y, Zhang Y, Zaun H-C, Karellis A, Koromilas AE,**
663 **Lipman ML, Karaplis AC.** Defective interplay between mTORC1 activity and

endoplasmic reticulum stress-unfolded protein response in uremic vascular calcification. *Am J Physiol Renal Physiol* 314: F1046-F1061, 2018. doi:10.1152/ajprenal.00350.2017.

30. **Patel JJ, Srivastava S, Siow RC.** Isolation, Culture, and Characterization of Vascular Smooth Muscle Cells. *Methods Mol Biol* 1430: 91-105, 2016. doi:10.1007/978-1-4939-3628-1_6.
31. **Proudfoot D, Skepper JN, Hegyi L, Bennett MR, Shanahan CM, Weissberg PL.** Apoptosis regulates human vascular calcification in vitro: evidence for initiation of vascular calcification by apoptotic bodies. *Circ Res* 87: 1055-1062, 2000. doi:10.1161/01.res.87.11.1055.
32. **Reid IR, Birstow SM, Bolland MJ.** Calcium and Cardiovascular Disease. *Endocrinol Metab (Seoul)* 32: 339-349, 2017. doi:10.3803/EnM.2017.32.3.339.
33. **Rodenbeck SD, Zarse CA, McKenney-Drake ML, Bruning RS, Sturek M, Chen NX, Moe SM.** Intracellular calcium increases in vascular smooth muscle cells with progression of chronic kidney disease in a rat model. *Nephrol Dial Transplant* 32: 450-458, 2016. doi:10.1093/ndt/gfw274.
34. **Shanahan CM, Crouthamel MH, Kapustin A, Giachelli CM.** Arterial calcification in chronic kidney disease: key roles for calcium and phosphate. *Circ Res* 109: 697-711, 2011. doi:10.1161/CIRCRESAHA.110.234914.
35. **Shroff RC, McNair R, Figg N, Skepper JN, Schurgers L, Gupta A, Hiorns M, Donald AE, Deanfield J, Rees L, Shanahan CM.** Dialysis accelerates medial vascular calcification in part by triggering smooth muscle cell apoptosis. *Circulation* 118: 1748-1757, 2008. doi:10.1161/circulationaha.108.783738.
36. **Speer MY, Yang H-Y, Brabb T, Leaf E, Look A, Lin W-L, Frutkin A, Dichek D,**

Giachelli CM. Smooth muscle cells give rise to osteochondrogenic precursors and chondrocytes in calcifying arteries. *Circ Res* 104: 733-741, 2009. doi:10.1161/CIRCRESAHA.108.183053.

37. **Speer MY, Yang HY, Brabb T, Leaf E, Look A, Lin WL, Frutkin A, Dichek D, Giachelli CM.** Smooth muscle cells give rise to osteochondrogenic precursors and chondrocytes in calcifying arteries. *Circ Res* 104: 733-741, 2009. doi:10.1161/circresaha.108.183053.
38. **Stevens KK, Patel RK, Mark PB, Delles C, Jardine AG.** Phosphate as a cardiovascular risk factor: effects on vascular and endothelial function. *Lancet* 385 Suppl 1: S10, 2015. doi:10.1016/s0140-6736(15)60325-7.
39. **Takeda E, Taketani Y, Morita K, Miyamoto K.** Sodium-dependent phosphate co-transporters. *Int J Biochem Cell Biol* 31: 377-381, 1999.
40. **Tonelli M, Sacks F, Pfeffer M, Gao Z, Curhan G.** Relation between serum phosphate level and cardiovascular event rate in people with coronary disease. *Circulation* 112: 2627-2633, 2005. doi:10.1161/circulationaha.105.553198.
41. **Toussaint ND, Pedagogos E, Tan SJ, Badve SV, Hawley CM, Perkovic V, Elder GJ.** Phosphate in early chronic kidney disease: associations with clinical outcomes and a target to reduce cardiovascular risk. *Nephrology (Carlton)* 17: 433-444, 2012. doi:10.1111/j.1440-1797.2012.01618.x.
42. **Trebak M, Ginnan R, Singer HA, Jourd'heuil D.** Interplay between calcium and reactive oxygen/nitrogen species: an essential paradigm for vascular smooth muscle signaling. *Antioxid Redox Signal* 12: 657-674, 2010. doi:10.1089/ars.2009.2842.
43. **Villa-Bellosta R, Bogaert YE, Levi M, Sorribas V.** Characterization of

712 phosphate transport in rat vascular smooth muscle cells: implications for
713 vascular calcification. *Arterioscler Thromb Vasc Biol* 27: 1030-1036, 2007.
714 doi:10.1161/atvbaha.106.132266.
715 44. **Wyatt CM, Drueke TB.** Vascular calcification in chronic kidney disease: here to
716 stay? *Kidney Int* 92: 276-278, 2017. doi:10.1016/j.kint.2017.05.019.
717 45. **Xu S, Kim JH, Hwang KH, Das R, Quan X, Nguyen TT, Kim SJ, Cha SK, Park**
718 **KS.** Autocrine insulin increases plasma membrane K(ATP) channel via PI3K-
719 VAMP2 pathway in MIN6 cells. *Biochem Biophys Res Commun* 468: 752-757,
720 2015. doi:10.1016/j.bbrc.2015.11.028.
721 46. **Yamada K, Fujimoto S, Nishiura R, Komatsu H, Tatsumoto M, Sato Y, Hara**
722 **S, Hisanaga S, Ochiai H, Nakao H, Eto T.** Risk factors of the progression of
723 abdominal aortic calcification in patients on chronic haemodialysis. *Nephrol Dial*
724 *Transplant* 22: 2032-2037, 2007. doi:10.1093/ndt/gfm031.
725 47. **Yamazaki M, Ozono K, Okada T, Tachikawa K, Kondou H, Ohata Y,**
726 **Michigami T.** Both FGF23 and extracellular phosphate activate Raf/MEK/ERK
727 pathway via FGF receptors in HEK293 cells. *J Cell Biochem* 111: 1210-1221,
728 2010. doi:10.1002/jcb.22842.
729 48. **Zhao Y, Zhao MM, Cai Y, Zheng MF, Sun WL, Zhang SY, Kong W, Gu J, Wang**
730 **X, Xu MJ.** Mammalian target of rapamycin signaling inhibition ameliorates
731 vascular calcification via Klotho upregulation. *Kidney Int* 88: 711-721, 2015.
732 doi:10.1038/ki.2015.160.
733 49. **Zoidis E, Ghirlanda-Keller C, Gosteli-Peter M, Zapf J, Schmid C.** Regulation
734 of phosphate (Pi) transport and NaPi-III transporter (Pit-1) mRNA in rat
735 osteoblasts. *J Endocrinol* 181: 531-540, 2004. doi:10.1677/joe.0.1810531.

FIGURE LEGENDS

Figure 1. High phosphate accelerates osteogenic differentiation and vascular calcification via ERK1/2-mTOR pathway. (A) Primary vascular smooth muscle cells (pVSMCs) isolated from rat thoracic aorta were treated with inorganic phosphate (Pi; 3 and 5 mM) for 2 days and calcification was detected by Alizarin staining (N=5). (B) pVSMCs were treated with 5 mM Pi for 24 h followed by western blotting to detect p-ERK1/2 and p-p70S6K (N=5). (C) Representative confocal images of pVSMCs showing the location of NF-κB (green) after 48 h Pi (5 mM) incubation (N=3). Cells were counterstained with DAPI (blue). (D) Real-time PCR was used to assess runt-related transcription factor 2 (Runx2, N=3) and osteopontin (OPN, N=4) expression in Pi (5 mM)-treated A7r5 cells with UO126 and rapamycin. (E) Western blot analysis for ER stress markers, PERK and CHOP. (F) Cell viability and apoptotic DNA fragmentation were estimated using MTT and cell death detection kit. (G, H, I) Alizarin staining was used to evaluate Pi-triggered calcification in pVSMCs (N=3) upon UO126 (10μM), Rapamycin (10nM) and Wogonin (5μM) treatment. Data represent mean ± standard error of the mean (SEM) and N is the number of independent experiments. *P*-values of one-way analysis of variance (ANOVA) are indicated at the top of the bar diagrams and *, **, ***, **** denotes $P < 0.05$, $P < 0.01$, $P < 0.001$ and $P < 0.0001$.

Figure 2. Increased protein abundance and surface trafficking of PiT-1/2 by high phosphate. (A) End-point RT-PCR and western blotting showing the

759 expression of sodium-phosphate cotransporters in pVSMCs. Rat kidney was used as
760 a positive control for NaPi-IIa and IIc. (B, C) Concentration-dependence (B; 24 h;
761 N=3) and time kinetics (C; 5 mM; N=3) of Pi-induced PiT-1/2 upregulation in A7r5
762 cells. (D, E) Effects of UO126 (D) and rapamycin (E) on upregulation of PiT-1/2
763 proteins after high Pi treatment for 24 h in A7r5 cells (N=3). (F, G) Concentration
764 dependence (F; 1 h) and time kinetics (G; 5 mM) of Pi-induced PiT-1 abundance
765 changes in the plasma membrane (surface) and cell lysates (lysate) measured by
766 biotinylation analysis and western blotting in A7r5 cells (N=3). (H) Effects of PiT-1
767 and -2 knockdown on Pi-induced calcification of pVSMCs were measured using
768 Alizarin staining (N=3). Data represent mean ± SEM and N is the number of
769 independent experiments. *P*-values of one-way ANOVA are indicated at the top of
770 the bar diagrams and *, **, **** denotes $P < 0.05$, $P < 0.01$, and $P < 0.0001$.

771

772 **Figure 3. Cytosolic Ca^{2+} increase is critical for phosphate-induced vascular**
773 **calcification.** (A) Changes in intracellular Ca^{2+} concentration ($[Ca^{2+}]_i$) by varying
774 levels of extracellular Pi in A7r5 cells seeded on black-walled 96-well plates and
775 measured by using Fura-2 with the multi-well FlexStation reader. Delta (Δ) Fura-2
776 ratio was calculated to indicate the magnitude of $[Ca^{2+}]_i$ changes (N=4). (B) Effects of
777 different extracellular Ca^{2+} concentrations on $[Ca^{2+}]_i$ in A7r5 cells by 5 mM Pi (N=3).
778 (C, D, E) Representative Immunoblotting of p-ERK1/2 (C, N=3), mRNA levels of
779 Runx2 and OPN (D, N=3), and calcific changes visualised with Alizarin staining (E,
780 N=3) were observed in A7r5 cells incubated in high Pi-containing medium with or
781 without extracellular Ca^{2+} or EGTA-AM. Data represent mean ± SEM and N is the
782 number of independent experiments. *P*-values of one-way ANOVA are indicated at

783 the top of the bar diagrams and ***, **** denotes $P < 0.001$, and $P < 0.0001$.

784

785 **Figure 4. High phosphate increases cytosolic Ca^{2+} by depolarization-activated**
786 **Ca^{2+} uptake.** (A) Changes in plasma membrane potential ($\Delta\Psi_p$) were detected by
787 using $DiBAC_4(3)$ fluorescence dye in A7r5 cells exposed to different concentrations
788 of K^+ solution. (B) Effects of 5 mM extracellular Pi on depolarization of $\Delta\Psi_p$ were
789 measured by confocal live cell imaging system and 30 mM KCl was used as a
790 positive control (N=3, n=52-60). (C) Effects of knockdown of PiT-1 only or PiT-1 and -
791 2 both on Pi-induced $\Delta\Psi_p$ depolarization in A7r5 cells (N=5, n=74-87). (D) In A7r5
792 cells, role of extracellular Na^+ on Pi-induced $[Ca^{2+}]_i$ increase. $[Ca^{2+}]_i$ changes was
793 monitored by multi-well FlexStation reader. Extracellular Na^+ free solution was
794 prepared by replacing Na^+ with NMDG in KRBB (N=4). (E) Effects of PiT-1/2
795 knockdown on Pi-induced $[Ca^{2+}]_i$ increase (N=3, n=27-30). (F) Effect of verapamil, an
796 inhibitor of voltage-gated Ca^{2+} channel on Pi-induced $[Ca^{2+}]_i$ increase in A7r5 cells
797 (N=3, n=23-30). (G-I) Protective effect of verapamil on Pi-induced ERK1/2
798 phosphorylation (G, N=3) upregulation of osteogenic genes, Runx2 and OPN (H,
799 N=3), and calcific changes visualised with Alizarin staining in A7r5 cells (I, N=3). All
800 data represent mean ± SD (E, F) or SEM (C, D, H, I). N is the number of
801 independent experiments and n is the number of analyzed cells. *P*-values of
802 unpaired *t*-test (E, F) or one-way ANOVA (C, D, H, I) are indicated at the top of the
803 bar diagrams and *, **, **** denotes $P < 0.05$, $P < 0.01$, and $P < 0.0001$.

804

805 **Figure 5. Oxidative stress is dependent on cytosolic Ca^{2+} elevation in**

phosphate-induced vascular calcification: (A-D) Effects of antioxidant NAC (3 mM; A, N=3, n=74-91), Catalase (10 units/ml; B, N=3, n=140-209), Ca^{2+}-free medium (C; N=3, n=102-116), EGTA-AM (2 μM; D; N=3, n=75-77) and Verapamil (10 μM; E; N=3, n=102-139) on Pi-induced cytosolic ROS generation in A7r5 cells. (F-H) Effects of NAC on ERK1/2 phosphorylation (F, N=3), upregulation of Runx2 and OPN (G, N=3) and calcific changes (H, N=4) by high Pi (5 mM) exposure. Data represent mean ± SD (A-F) or SEM (G, H). N is the number of independent experiments and n is the number of analyzed cells. *P*-values of one-way ANOVA are indicated at the top of the bar diagrams and **** denotes $P < 0.0001$.

Figure 6. Mitochondrial superoxide scavenger effectively prevents phosphate-induced vascular calcification. (A) Representative trace of mitochondrial membrane potential ($\Delta\Psi_m$) of permeabilized A7r5 cells measured by using 300nM of JC-1 fluorescence dye. Extramitochondrial Pi increased JC-1 ratio, reflecting hyperpolarisation of $\Delta\Psi_m$ (N=3). (B) In A7r5 cells, mitochondrial superoxide production measured by using mitoSOX fluorescence dye (N=2, n=11-20). (C) Pi-induced superoxide production was prevented by pretreatment of mitoTEMPO (mtTP, 100 nM), a mitochondrial superoxide scavenger (N=3, n=36-39). (D) Representative confocal images of NF-κB (green) translocation in pVSMCs by 5 mM Pi exposure with or without mtTP pretreatment (N=3). Cells were counterstained with DAPI (blue). (E-G) Effects of mtTP (100 nM) on Pi-induced upregulation of PiT-1 total protein and ERK1/2 phosphorylation (E, N=3), transcriptional activation of Runx2 and OPN (F, N=4) and calcium deposition (G) in pVSMCs. Data represent mean ± SD (B, C) or mean ± SEM (F, G). (H) The diagram depicts high extracellular phosphate (Pi)

activates ERK and mTOR resulting in ER stress and apoptosis of VSMCs. High Pi depolarizes plasma membrane potential ($\Delta\Psi_p$) via PiT-1 and -2, then subsequently opens voltage-gated Ca^{2+} channels allowing intracellular Ca^{2+} elevation. Both cytosolic Ca^{2+} and Pi increases are responsible for oxidative stress and nuclear translocation of NF-κB, turning on osteoblast differentiation. Elevated Pi upregulates total proteins of PiT-1/2 via ERK1/2-mTOR and their surface trafficking. N is the number of independent experiments and n is the number of analyzed cells. *P*-values of one-way ANOVA analysis are indicated at the top of the bar diagrams. *, **, **** denotes $P < 0.05$, $P < 0.01$ and $P < 0.0001$.

[Supplemental Materials]

Supplementary Figure S1: https://doi.org/10.6084/m9.figshare.12732317

Supplementary Figure S2: https://doi.org/10.6084/m9.figshare.12732326

Supplementary Figure S3: https://doi.org/10.6084/m9.figshare.12732347

Supplementary Figure S4: https://doi.org/10.6084/m9.figshare.13019528

Supplementary Figure S5: https://doi.org/10.6084/m9.figshare.12733214

Supplementary Figure S6: https://doi.org/10.6084/m9.figshare.12733226

Supplementary Table 1: https://doi.org/10.6084/m9.figshare.12732368

Figure 1. Nguyen et al.

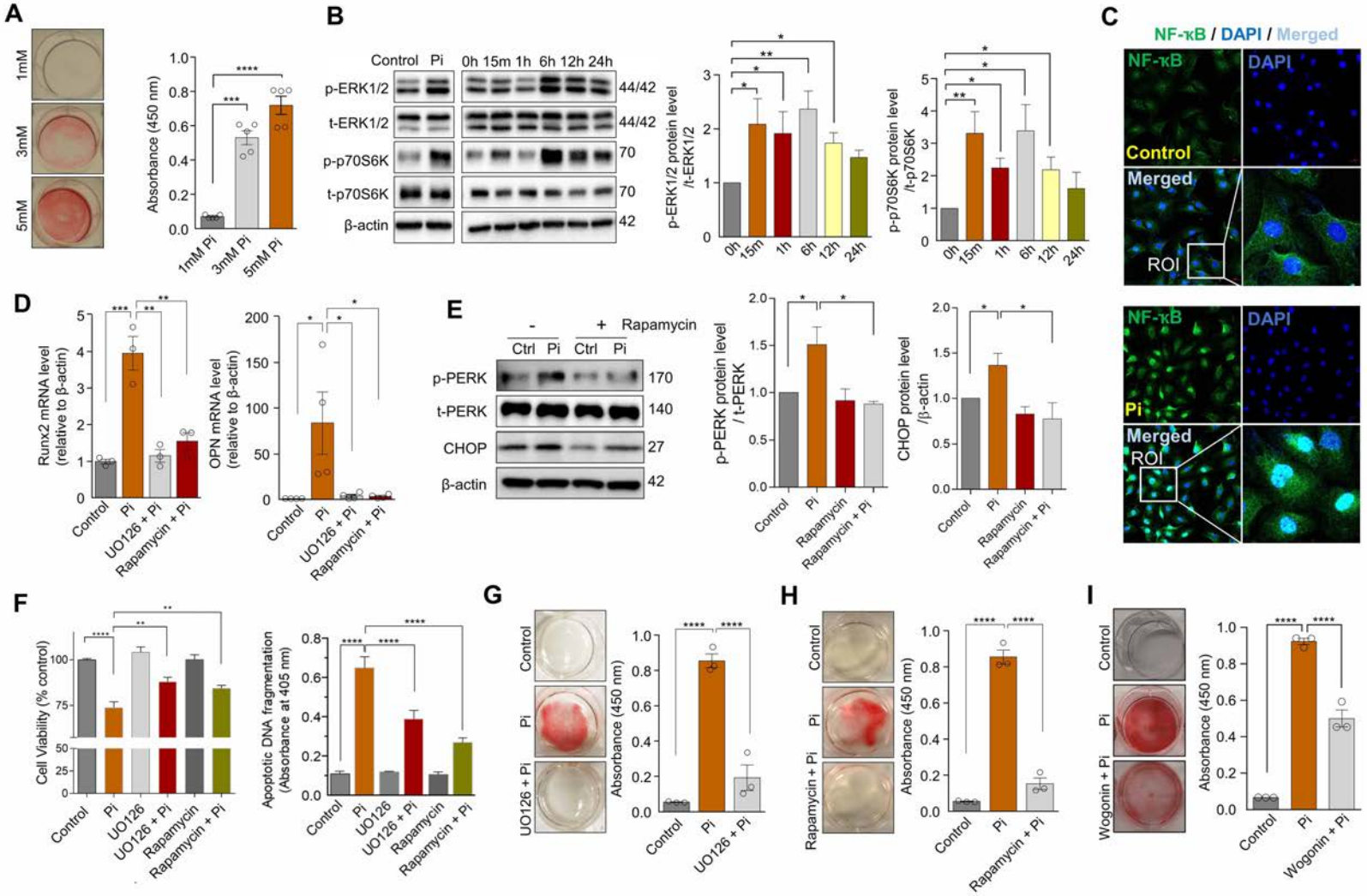

Figure 2. Nguyen et al.

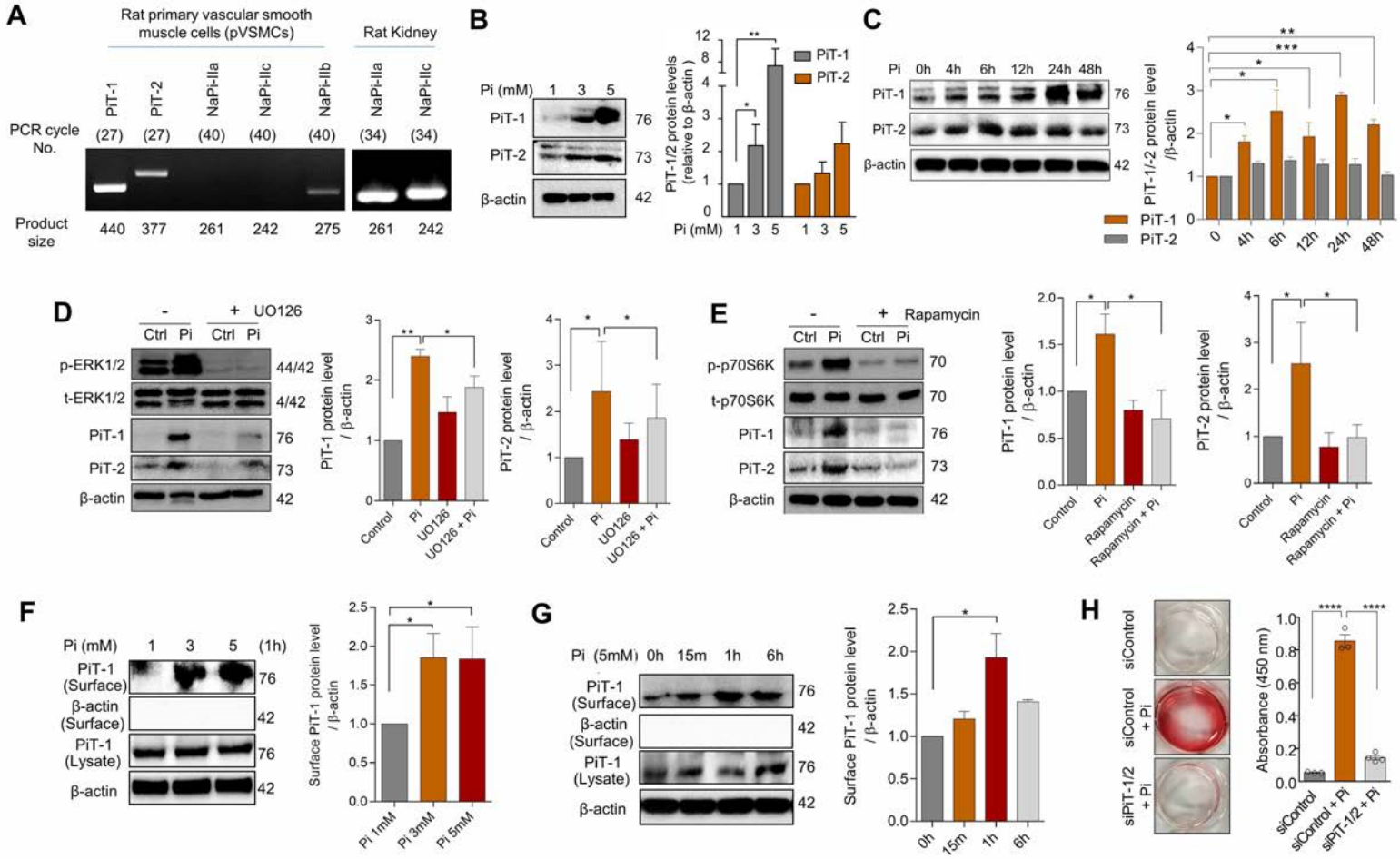

Figure 3. Nguyen et al.

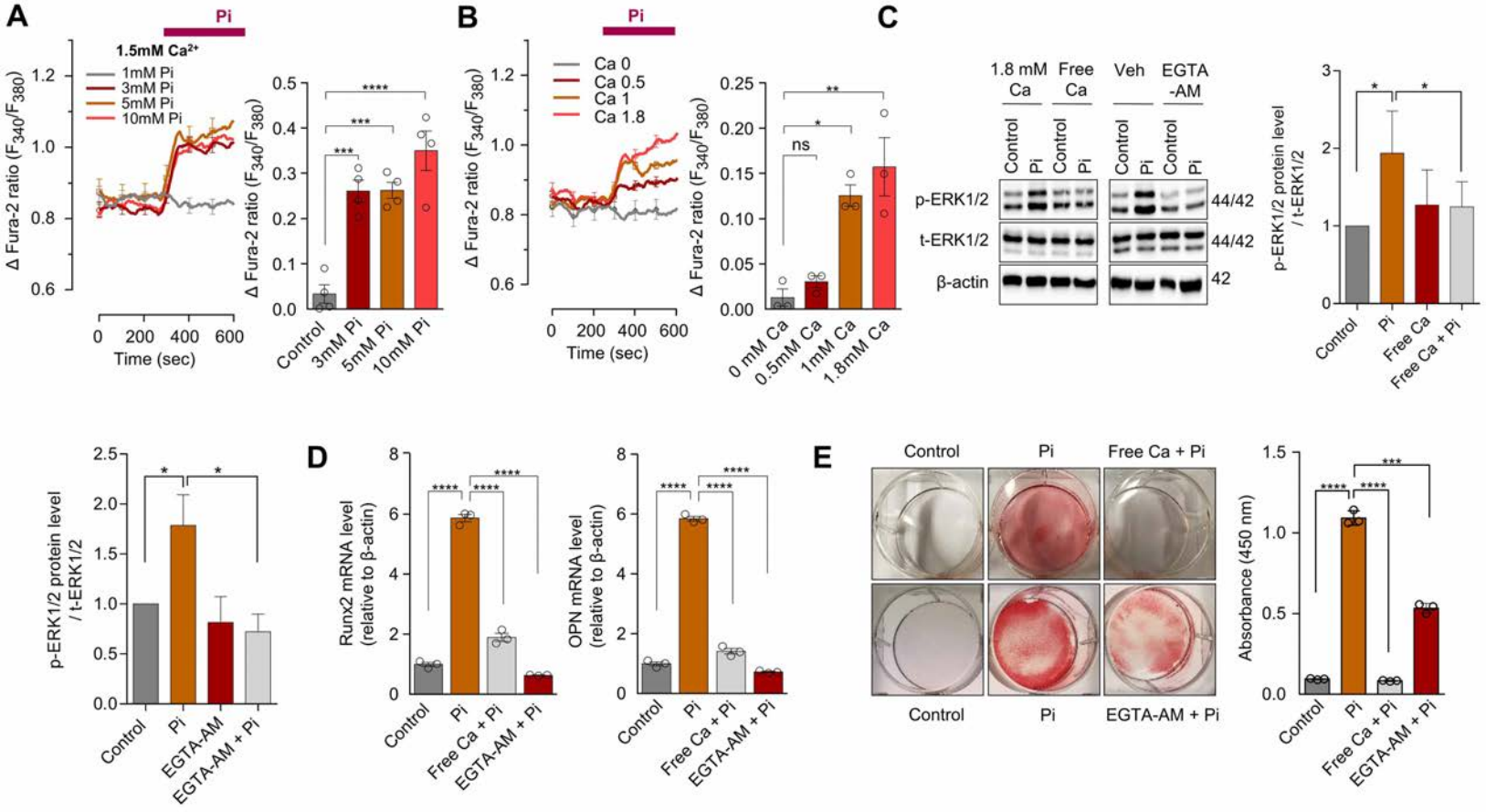

Figure 4. Nguyen et al.

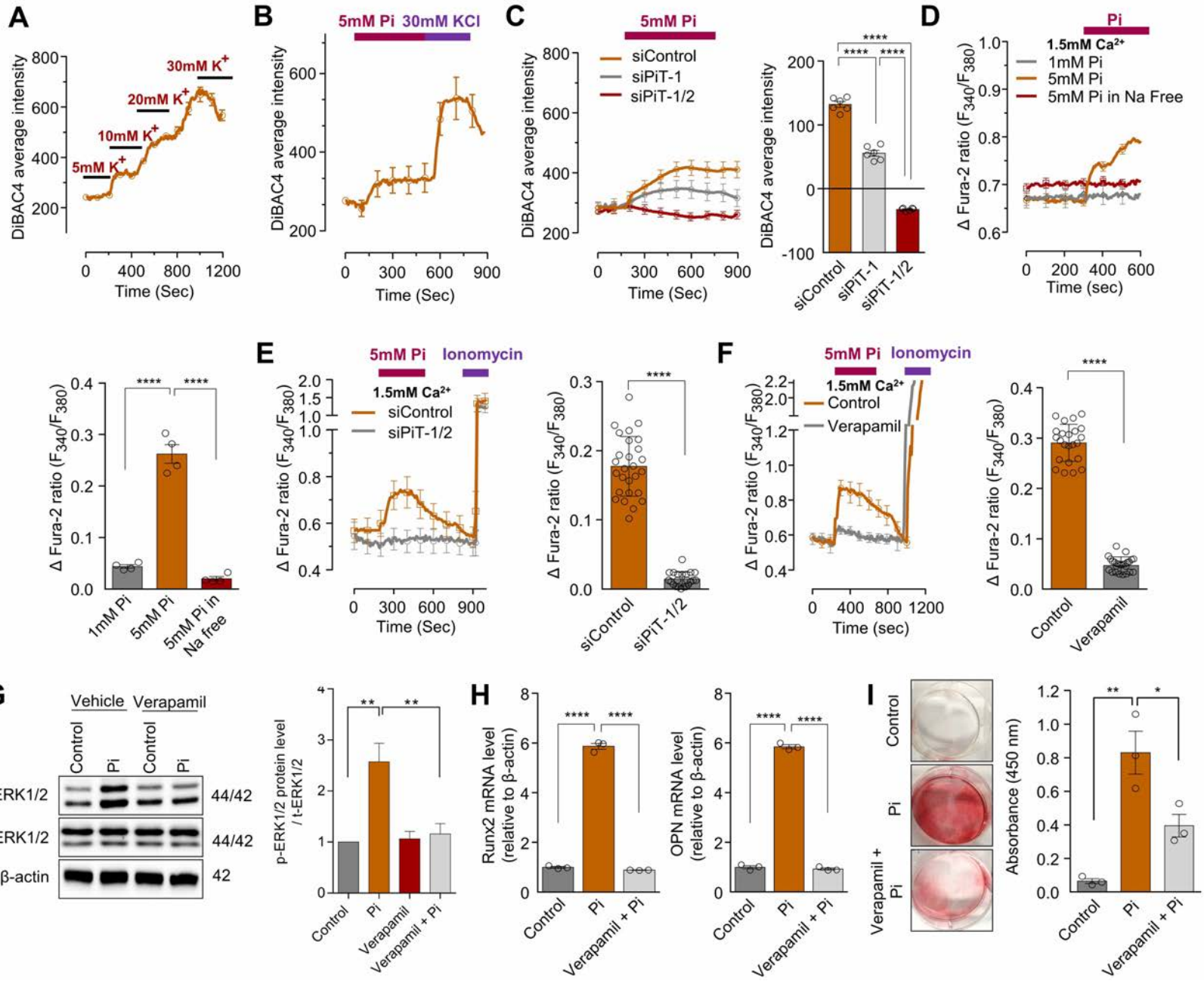

Figure 5. Nguyen et al.

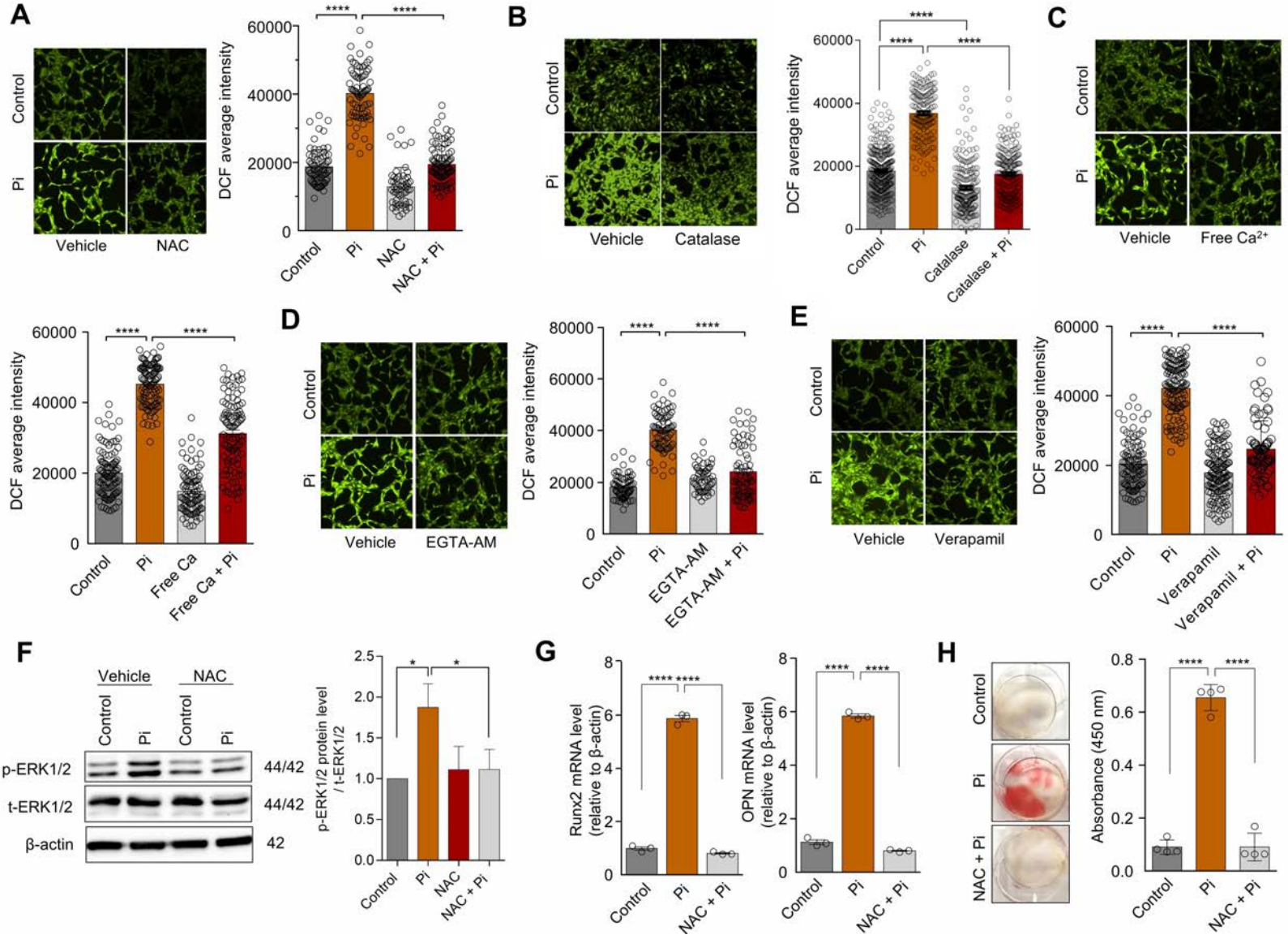

Figure 6. Nguyen et al.